Interannual variability of summer biochemical enhancement in relation to mesoscale eddies at the shelf break in the vicinity of the Pribilof Islands, Bering Sea

Kohei Mizobata [a,*], Sei-ichi Saitoh [c], Jia Wang [b,1]

[a] Department of Ocean Sciences, Tokyo University of Marine Science and Technology, 4-5-7 Kounan, Minato-ku, Tokyo 108-8477, Japan
[b] Arctic Modeling Group, International Arctic Research Center, University of Alaska Fairbanks, 930 Koyukuk Drive, Fairbanks, AK 99775-7335, USA
[c] Laboratory of Marine Bioresource and Environment Sensing, Graduate School of Fisheries Sciences, Hokkaido University, 3-1-1 Minato-cho, Hakodate, Hokkaido 041-8611, Japan

ARTICLE INFO

ABSTRACT

This study examined variability of the eddy field and primary production over the Bering Sea's eastern shelf break area during summer using a satellite multi-sensor data set. The eddy field and on-shelf nutrient flux below 50 m water depth were also investigated using a numerical model. The satellite-altimeter data analysis and numerical experiments indicated that the eddy field was induced by perturbations of the Bering Slope Current system and/or instabilities in the Bering Sea basin via flow through the Aleutian passes. The distribution of high primary production roughly coincided with the high variability area of the eddy field. Numerical experiments showed a 70% increase in net on-shelf flux and 54% increase in net on-shelf transport by the generation/propagation of eddies along the shelf break. At Pribilof Canyon, towed CTD/fluorometer measurements during the summer of 2003 revealed a stable water column and high fluorescence ($>10 \mu g L^{-1}$) in the area between the 200- and 1000-m isobaths at a time when there was a low level of on-shelf flux regardless of the eddy field. Conversely, the eddy-induced, on-shelf flux and stable water column can enhance primary production from spring to summer at the shelf break. Moreover, the eddy-induced on-shelf nutrient flux probably contributes to the primary productivity at the western shelf of the Pribilof Islands where the Bering Sea ecosystem is very dynamic. This eddy-related shelf break process can be applied to not only the Bering Sea shelf break but also all shelf break areas in which propagating eddies are found.

© 2008 Elsevier Ltd. All rights reserved.

1. Introduction

The Bering Sea is divided into the shallow continental shelf and the deep basin. In the deep basin, there are three major boundary currents, the Aleutian North Slope Current (ANSC; Reed and Stabeno, 1999), the Bering Slope Current (BSC; Kinder et al., 1975), and the Kamchatka Current. The ANSC turns northwestward near Umnak Plateau to feed the BSC (Stabeno et al., 1999). The BSC flows along the 1300-km-long eastern shelf break accompanied by a mesoscale eddy field (Okkonen, 2001a). Eddies occur with horizontal scales ranging from ~10 to 200 km along the Bering Sea shelf break (Stabeno et al., 1999). Along the eastern shelf break, previous altimeter analyses revealed that the evolution of the BSC eddy field begins in the spring and lasts through the summer (Okkonen, 2001a). During summer, one of the prominent features over the shelf break is the shedding of anticyclonic eddies (Mizobata and Saitoh, 2004). Eddies with a diameter of about 100 km often were observed by ship survey at the shelf break (Sapozhnikov, 1993; Mizobata et al., 2002). Mesoscale eddies, which penetrate to depths of at least 1000 m (Roden, 1995; Mizobata et al., 2002; Johnson et al., 2004), propagate northwestward along the shelf break or remain near Pribilof Canyon or Zhemchug Canyon (Okkonen, 2001a; Mizobata and Saitoh, 2004).

Because of its high productivity, the Bering Sea shelf break is called "the Bering Sea Green Belt" (Springer et al., 1996). Primary production at the shelf break starts to rise during the spring and increases throughout summer when the eddy field is developing. Previous studies showed high chlorophyll a (chl-a) distributions associated with mesoscale eddies in the Bering Sea (Sapozhnikov, 1993; Mizobata et al., 2002; Mizobata and Saitoh, 2004; Okkonen et al., 2004). In the western Bering Sea, Sapozhnikov (1993) revealed a renewal of water in the oxygen minimum layer and upwelling of deep water by strong anticyclonic eddies. He suggested that the intensity of eddy formation affects annual

* Corresponding author.
E-mail addresses: mizobata@kaiyodai.ac.jp (K. Mizobata), ssaitoh@salmon.fish.hokudai.ac.jp (S.-i. Saitoh), jwang@iarc.uaf.edu, jia.wang@noaa.gov (J. Wang).
[1] Present address: NOAA/GLERL, 2205 Commonwealth Boulevard, Ann Arbor, MI 48105, USA.

primary production and the quantity of nutrients. At the eastern Bering Sea shelf break, Mizobata et al. (2002) observed a cyclonic eddy and an anticyclonic eddy. Their hydrographic observations captured uplifted isopycnals indicating upwelling of nutrient-rich water inside eddies (Wang and Ikeda, 1997b). They measured relatively high chl-a distributions (1–2 mg m^{-3}) above the uplifted isopycnals around the periphery of an anticyclonic eddy and at the center of a cyclonic eddy. Using a satellite data set, Mizobata and Saitoh (2004) reported the interannual variability of the eddy field and primary production. They discussed a positive correlation along the TOPEX/Poseidon altimeter orbit between the variability of the eddy field and primary production, suggesting it occurred because of vertical eddy nutrient supply to the sub-surface layer. However, the causes of interannual variability in the eddy field remain largely unresolved. There is uncertainty in the correlation of the eddy field with primary productivity due to a limited data set. Additionally, the Bering Sea shelf break and basin are high-nutrient, low-chlorophyll areas. Therefore, vertical nutrient supply is not enough to explain the high and prolonged (from spring to summer) productivity of the shelf break. Okkonen et al. (2004) showed high chl-a concentrations associated with an anticyclonic eddy during spring, and they suggested that eddies can entrain chlorophyll and discharge it to the basin. This process could be important for the Bering Sea Green Belt that blooms from spring to summer.

Thus, the on-shelf flux associated with eddies is now hypothesized to be one of the mechanisms transporting nutrients and biota to the shelf break and shelf region (Stabeno et al., 1999; Okkonen, 2001a). Previous drifting buoy studies revealed the relationship between on-shelf flux and an eddy at the south shelf break of Pribilof Canyon (Schumacher and Stabeno, 1994; Stabeno and van Meurs, 1999). In the summer of 2001, an eddy-like feature and on-shelf flux also were observed at the shelf break west of the Pribilof Islands by a drifting buoy (Mizobata and Saitoh, 2003). Because drifting buoys measure only the surface flow between ~ 15 and 50 m, depending on the depth of a drifter's drogue, these studies do not provide complete information about eddies and on-shelf fluxes.

Thus, we need to clarify the roles and dynamics of mechanisms that maintain high productivity over the shelf break, including the effects of eddies and related on-shelf fluxes. The shelf break near the Pribilof Islands deserves examination because of a major nursery area for age-0 walleye pollock, which is an important forage fish of the Bering Sea ecosystem (Ciannelli et al., 2002; Swartzman et al., 2002). To further examine this hypothesis, we describe details of data sets and analyses that we used. We then investigate interannual variability of the eddy field and primary production at the shelf break and in the basin using a satellite data set. In addition, we present results from a numerical simulation of the on-shelf flux below 50 m water depth induced by mesoscale eddies at the shelf break. Finally, we provide results from a CTD/fluorometer towed at Pribilof Canyon in 2003.

2. Data and methods

2.1. Sea level anomalies

To examine the summer eddy field in the Bering Sea shelf break area, we employed the $1/3°$ Mercator gridded weekly merged sea-level anomalies (SLAs) data set from 1998 to 2003. This data set is distributed by archiving, validation and interpretation of Satellite Oceanographic data (AVISO, http://www.jason.oceanobs.com/html/donnees/produits/delai_uk.html). SLAs utilized in this study were merged from four satellite missions (TOPEX/Poseidon, ERS-1/2, Jason-1 and ENVISAT) using the optimum interpolation technique (Le Traon et al., 1998). These SLA maps have the same resolution in longitude and latitude directions (e.g., about 21.2 km at $55°$N). Therefore, the horizontal resolution of SLA maps is sufficient to investigate mesoscale eddies with horizontal scales from 100 to 200 km. In this study, SLAs over the shelf region (< 200 m water depth) were neglected due to inaccurate tide corrections. The geostrophic current and eddy kinetic energy (EKE) were estimated using SLAs and assuming geostrophic balance (Robinson, 2004):

$$u' = \frac{g}{f}\frac{\partial \text{SLA}}{\partial y}, \qquad v' = -\frac{g}{f}\frac{\partial \text{SLA}}{\partial x}, \tag{1}$$

$$\text{EKE} = \tfrac{1}{2}(u'^2 + v'^2). \tag{2}$$

Then, we computed standard deviations of EKE during each summer (July–September) at a given point using the mean EKE during each summer at that point by Eq. (2). Standard deviations of EKE during each summer are changed by the passage or the formation of mesoscale eddies. In this study, we reveal the variability of the BSC eddy field using these standard deviations of EKE.

2.2. Primary production

Summer primary production from 1998 to 2003 was derived from maps of sea-surface temperature (SST), chl-a and photosynthetically active radiation (PAR). Sources for these estimates were, respectively, NOAA/AVHRR Pathfinder Sea Surface Temperature version.5, the Sea-viewing Wide Field-of-view Sensor (SeaWiFS) derived chl-a and SeaWiFS PAR. The horizontal and time resolutions of SST, chl-a and PAR maps were 9 km and 1 month. SeaWiFS chl-a was derived from the Global standard algorithm, Ocean Color 4 version 4 (O'Reilly et al., 2000) using the SeaWiFS Data Analysis System version 4.7 distributed by the NASA/Goddard Space Flight Center OceanColor website (http://oceancolor.gsfc.nasa.gov/seadas/download.html). The primary production field was estimated using the Vertically Generalized Production Model (VGPM; Behrenfeld and Falkowski, 1997), modified by the two-phytoplankton community model (Kameda and Ishizaka, 2005). Details of the VGPM and Kameda–Ishizaka model are given in Behrenfeld and Falkowski (1997) and Kameda and Ishizaka (2005). The Behrenfeld and Falkowski's VGPM estimates the depth-integrated primary production in the euphotic zone (PP_{eu}) with the optimal rate of carbon fixation within the water column, called $P_{\text{opt}}^{\text{B}}$:

$$PP_{\text{eu}} = \text{Chl}_{\text{surf}} \times Z_{\text{eu}} \times P_{\text{opt}}^{\text{B}} \times \text{DL}$$
$$\times \left[0.66125 \times \frac{E_0}{E_0 + 4.1} \right] \tag{3}$$

$$Z_{\text{eu}} = \begin{cases} 568.2(C_{\text{tot}})^{-0.746} & \text{if } Z_{\text{eu}} < 102 \\ 200.0(C_{\text{tot}})^{-0.293} & \text{if } Z_{\text{eu}} > 102 \end{cases} \tag{4}$$

$$C_{\text{tot}} = \begin{cases} 38.0(C_{\text{surf}})^{0.425} & \text{if } C_{\text{surf}} < 1.0 \\ 40.2(C_{\text{surf}})^{0.507} & \text{if } C_{\text{surf}} \geqslant 1.0 \end{cases} \tag{5}$$

where Chl_{surf} is the SeaWiFS chl-a, DL is day length (or photoperiod) in decimal hours, Z_{eu} is the physical depth of the euphotic zone defined as the penetration depth of 1% of surface irradiance. This Z_{eu} is calculated from Chl_{surf} based on the Beer–Lambert law (Morel and Berthon, 1989; Eqs. (4) and (5)). E_0 is SeaWiFS Level 3 PAR. $P_{\text{opt}}^{\text{B}}$ of the original VGPM is derived from a seventh-order polynomial function of

SST (°C):

$$P_{\text{opt}}^{\text{B}} = 1.2956 + 2.749 \times 10^{-1}T + 6.17 \times 10^{-2}T^2 - 2.05$$
$$\times 10^{-2}T^3 + 2.462 \times 10^{-3}T^4 - 1.348 \times 10^{-4}T^5$$
$$+ 3.4132 \times 10^{-6}T^6 - 3.27 \times 10^{-8}T^7, \quad (6)$$

where T is SST. Kameda and Ishizaka (2005) pointed out that $P_{\text{opt}}^{\text{B}}$ (Eq. (6)) with its high variance tends to overestimate or underestimate PP_{eu}, and they modified this function based on two assumptions: (1) the change of large-sized phytoplankton abundance varies with chl-a value, and (2) chl-specific productivity of phytoplankton tends to be inversely proportional to phytoplankton size. In the Bering Sea, we must consider the various sizes and species of phytoplankton (Sukahanova et al., 1999; Shiomoto et al., 2002; Liu et al., 2002). The modified $P_{\text{opt}}^{\text{B}}$ by Kameda and Ishizaka (2005) is derived from AVHRR SST and SeaWiFS chl-a:

$$P_{\text{opt}}^{\text{B}} = \frac{0.071 \times T - 3.2 \times 10^{-3}T^2 + 3.0 \times 10^{-5}T^3}{\text{Chl}_{\text{surf}} + (1.0 + 0.17 \times T - 2.5 \times 10^{-3}T^2 - 8.0 \times 10^{-5}T^3)}. \quad (7)$$

In this study, we calculated the summer-averaged (July–September) PP_{eu} in the Bering Sea, which was compared to the variability of the eddy field described in Section 2.1. It should be noticed that the SeaWiFS monthly 9-km-averaged images (chl-a and PAR) in the Bering Sea will have uncertainties due to lack of skyward radiance data resulting from heavy cloud cover. However, the summer chl-a in the Bering Sea shelf break does not show an abrupt increase, unlike the spring bloom. Also, we focus on the mesoscale processes characterized at ~100–200 km horizontal scales. Therefore, it is worthwhile to investigate the potential primary production field during summer in the Bering Sea using monthly images. The daily-scale (or further short-scale) and small-scale variability of PP_{eu} are beyond the scope of this study.

2.3. Estuarine coastal and ocean model with semi-implicit and predictor–corrector schemes

To simulate the BSC eddy field and associated on-shelf fluxes, we applied a modified version (Wang and Ikeda, 1997a) of the Estuarine Coastal and Ocean Model with semi-implicit scheme (ECOM-si; Blumberg, 1991). ECOM-si has the following features: horizontal curvilinear coordinates and sigma vertical coordinates, the Arakawa-C grid (Arakawa and Lamb, 1977), a free surface, no time-splitting between the internal and external modes, and a second-order turbulence closure model for vertical viscosity (Mellor and Yamada, 1982). A semi-implicit scheme is introduced for solving the surface elevation in the shallow-water equations (Casulli, 1990). The difference between the ECOM-si used here and the original version (Blumberg, 1991) is a predictor–corrector scheme (Wang and Ikeda, 1995, 1997a). The use of a predictor–corrector scheme allows removal of an inertial instability introduced by the Euler forward scheme in time, and simulation of unstable waves and eddies in a very low viscosity environment (Wang and Ikeda, 1997c).

The simulation area is 100×100 horizontal grid points ($500\,\text{km} \times 500\,\text{km}$) covering the shelf break in the vicinity of the Pribilof Islands, with open southeastern and northwestern boundaries (Fig. 1). The orientations of x- and y-axes are southeast and northeast, respectively. The horizontal resolution of this model is $5\,\text{km} \times 5\,\text{km}$, which is less than half the internal baroclinic Rossby radius of deformation (Rd), estimated to be about 10.67 km at 58°N. Twenty-one sigma vertical levels ($\sigma = 0.0$, -0.04, -0.08, -0.115, -0.15, -0.185, -0.22, -0.255, -0.29, -0.33, -0.4, -0.47, -0.54, -0.61, -0.68, -0.75, -0.8, -0.85, -0.9, -1.0)
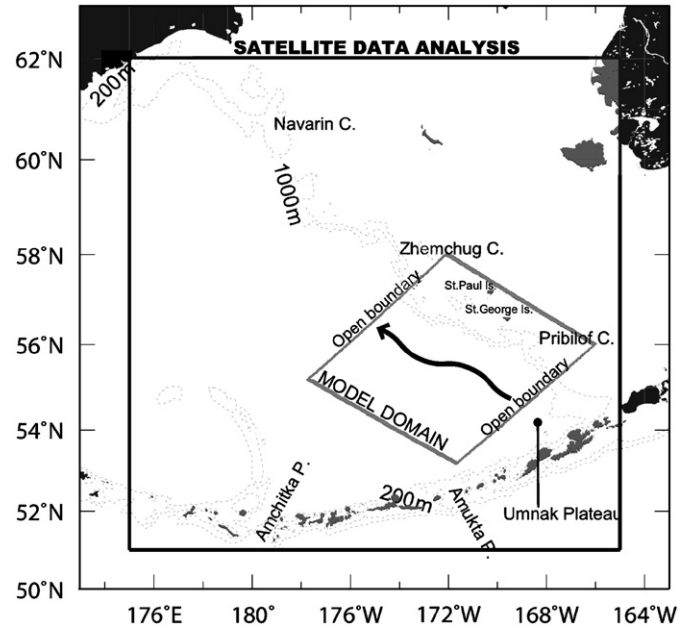

Fig. 1. The eastern Bering Sea and the model domain: dashed lines represent the 200- and 1000-m isobaths. The solid square shows the study area for the satellite data analysis. The model domain (gray square) covers the shelf break area in the vicinity of the Pribilof Islands (St. Paul Island and St. George Island).

were used. Bathymetry information was prepared using a 5-min ETOPO global elevation model.

Our numerical experiments did not use spin-up integration. To simulate the BSC and eddy field, we specified cross-slope isopycnals tilts at the shelf break in this model, based on our field temperature and salinity measurements. The isopycnal tilt has the opposite orientation to the continental shelf slope (Wang and Ikeda, 1997a; Mizobata et al., 2006). At the open boundary, in situ temperature and salinity vertical profiles, obtained by CTD (conductivity, temperature, depth) on Hokkaido University's T/S *Oshoro-maru* in 2001, were applied.

According to Mizobata et al. (2006), an optimum mechanism for the development of mesoscale eddies is jet flow. For the BSC, the "jet" or central axis of the current is located 50 km from the shelf break, and has a barotropic wavelength of 200 km along the continental slope, as determined from 44 sensitivity experiments. A distance of 50 km from the shelf break is plausible because Johnson et al. (2004) has revealed the signature of the BSC between 30 and 50 km offshore from the 1000-m isobath.

To clarify the effects of the eddy field on the on-shelf flux, we ran the ECOM-si from initial conditions with and without a barotropic perturbation of 200-km wavelength. Following Wang and Ikeda (1997b), we applied the following "external perturbation" to temperature and salinity fields:

$$0.1 \sin\left(\frac{2\pi}{L_x}x\right) \exp\left[-\left(\frac{y - y_0}{a}\right)^2\right], \quad (8)$$

where y_0 is the location of the front ($Y = 250\,\text{km}$), a equals $1.8\text{Rd} = 19.21\,\text{km}$, and L_x is 200 km. A perturbation of this wavelength was assumed to be triggered where the ANSC turns northwestward, feeding the BSC. Effective horizontal eddy viscosity and diffusivity were calculated using Smagorinsky's (1963) formulation, and effective vertical eddy viscosity and diffusivity were calculated by a second-order turbulent closure scheme (Mellor and Yamada, 1982). Using the semi-implicit scheme, the time step is 120 s, which is 6 times the Courant–Friedrichs–Levy Condition (CFL) (Wang, 1996). The model was integrated to 40 days.

We also conducted simultaneous numerical tracer experiments for on-shelf fluxes related to the eddy field. A non-dimensional passive tracer was introduced beneath $\sigma = -0.115$ over the deep basin (> 1000 m water depth). A tracer concentration of each grid is assumed 20 for nitrate–nitrite concentration in the basin area. After simulating the eddy field, we calculated the integrated, on-/off-shelf fluxes between 50–200 and 0–50 m water depth along the 200-m isobath using the following formula:

$$\text{Flux} = \int_{50\,\text{m}}^{200\,\text{m}} CV \, dx \, dz \quad \text{and} \quad \int_{0\,\text{m}}^{50\,\text{m}} CV \, dx \, dz, \qquad (9)$$

where C is tracer concentration (μM), V is on-shelf velocity (m s^{-1}), dx is the horizontal scale of the model grid (5000 m) and dz is the vertical grid size (m). Using Eq. (9), we integrated tracer flux, $CV \, dx \, dz$, from $\sigma = -0.255$ to -1.0 and $\sigma = 0.0$ to -0.255 corresponding to water depths ≈ 50–200 and 0–50 m at the 200-m isobath, respectively. In the Bering Sea shelf, there is low nutrient concentration in the surface layer (0–50 m), while high concentration of major nutrients can be found below 50 m water depth. Estimation of on-/off-shelf fluxes between 0–50 and 50–200 m water depth allows us to infer how the origin of nutrients occurs.

2.4. Hydrographic observations using a towed undulating vehicle

AVISO SLA maps show that two mesoscale anticyclonic eddies propagated along the eastern shelf break near Pribilof Canyon from 2 July to 19 November in 2003 (not shown). Hydrographic measurements conducted by Hokkaido University's T/S *Oshoro-maru* at Pribilof Canyon on 26 July 2003, documented the three-dimensional structure of temperature and fluorescence during this period. To acquire oceanic variable parameters at the shelf break, we employed an Nv-shuttle towed undulating vehicle developed by Chelsea Technologies Group. The Nv-shuttle can undulate by manipulation of the vehicle's impellor-driven alternator while it makes observations. A MINI$^{\text{pack}}$ CTD-F sensor suite and FAST $^{\text{tracka}}$ I fast repetition rate fluorometer were installed in the Nv-shuttle. The accuracy/resolution of temperature derived from the MINI$^{\text{pack}}$ CTD-F sensor suite was 0.003/0.0005 °C. The sensitivity of the FAST $^{\text{tracka}}$ I fast repetition rate fluorometer was 0.1–30 μg L^{-1}. Salinity measured by the MINI$^{\text{pack}}$ CTD-F was not applied in this study, because of suspicion of large errors.
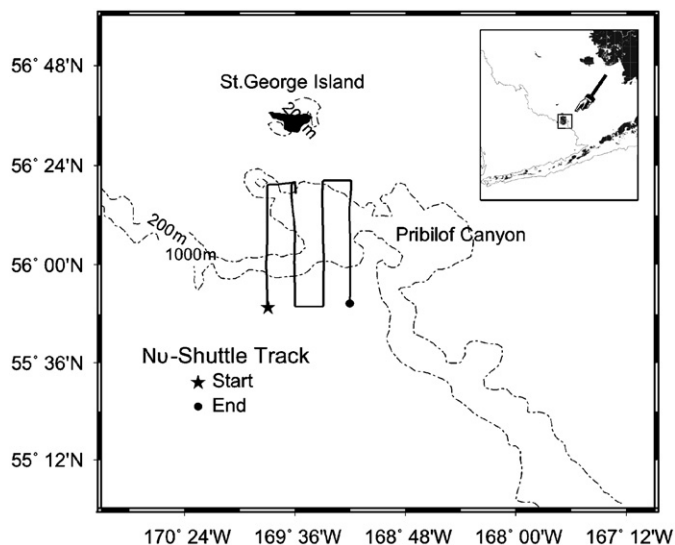

Fig. 2. Cruise track of the T/S *Oshoro-maru* (Faculty of Fisheries, Hokkaido University) for the 3-D hydrographic survey using a towed undulating vehicle on 26 July 2003.

We deployed the Nv-shuttle at 55.83°N, 169.8°W and towed it behind the T/S *Oshoro-maru* along the survey track at speeds of about nine knots (Fig. 2). The distance between each transect was about 12.4 km. Data were obtained between 10 and 60 m water depth, including the thermocline.

3. Results

3.1. Interannual variability of the summer eddy field

The spatial distribution of variability in the eddy field each summer was successfully determined using SLAs from 1998 to 2003 (Fig. 3). Large standard deviations of EKE were caused by propagating eddies or the formation/decay of eddies. The high eddy activity area was roughly consistent with where the BSC flows. Although some regions seemed routinely to have high EKE, there was still significant interannual variability of the eddy field over the six-summer period.

In 1998, high variability in the eddy field was found along the eastern shelf break and the north side of the Aleutian Islands (Fig. 3A). Mesoscale eddies were mainly generated south of Pribilof Canyon and along the eastern shelf break. The lowest variability of EKE (< 30 cm^2 s^{-2}) was found at $\sim$55–56°N, 174°W near the Zhemchug Canyon, implying that eddies generated south of Pribilof Canyon tended to remain there or weak eddies occur and dissipate there. Along the Aleutian Islands, high EKE variability with a maximum value of 197 cm^2 s^{-2} was generated near Amchitka Pass (52.7°N, 176.3°W). High EKE variability with a maximum value of 187 cm^2 s^{-2} was also evident over Umnak Plateau (53.5°N, 171.0°W).

The EKE standard deviation map for 1999 (Fig. 3B) shows less variability than in 1998. Relatively high eddy activity appeared near Pribilof Canyon, Zhemchug Canyon and along the Aleutian Islands, reaching a maximum EKE variability of 100 cm^2 s^{-2} (54.8°N, 171.3°W), 112 cm^2 s^{-2} (57.8°N, 177.6°W), and 110 cm^2 s^{-2} (52.3°N, 176.6°W), respectively. High variability near the eastern shelf break at 54–56°N, 172.5–170°W and low EKE variability south of Pribilof Canyon and Zhemchug Canyon suggest that eddies remained there. Moreover, little variability in the eddy field (< 10 cm^2 s^{-2}) was shown between Pribilof Canyon and Zhemchug Canyon. This suggests that there was no mesoscale eddy propagation between Pribilof Canyon and Zhemchug Canyon during summer. Along the Aleutian Islands, a narrow band of high EKE variability of more than 30 cm^2 s^{-2} occurred.

From 2000 to 2003, variability of the eddy field was high (30–120 cm^2 s^{-2}) along the shelf break from Umnak Plateau to Navarin Canyon (Fig. 3C–F). In 2000, a band of high EKE variability along the eastern shelf break had a width of about 130 km from shelf break to basin (Fig. 3C), suggesting the generation of the eddy field and northwestward propagation. A band of high EKE variability of that width is reasonable compared to the size of Bering Sea eddies (Mizobata et al., 2002). Recirculation with offshore movement of the eddy field was implied at 56°N, 174°W. Along the Aleutian Islands, high eddy activity is evident between Amchitka Pass and Amukta Pass.

In 2001 (Fig. 3D), relatively low EKE variability (< 80 cm^2 s^{-2}) was found along the eastern shelf break near Pribilof Canyon, with a thin band ($\sim$90-km wide from shelf break to basin) of high eddy activity. Thus, slightly smaller scale eddies propagated in the vicinity of Pribilof Canyon in the summer of 2001. From Zhemchug Canyon to Navarin Canyon, high eddy activity suggests a broad, propagating wave train. Fig. 3D shows two noticeable broad distributions ranging from Amchitka Pass to the deep basin at 52–55°N, 180–176°W and 53–55°N,
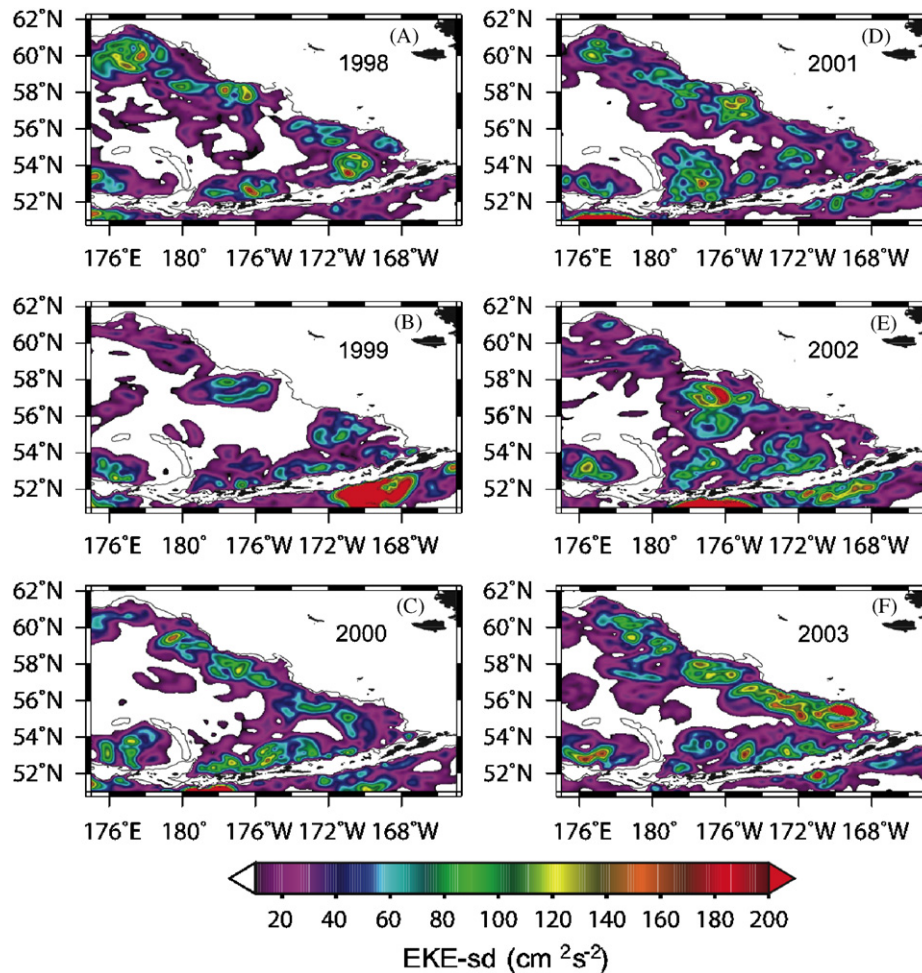
Fig. 3. Variability of the summer eddy field in the eastern Bering Sea; this figure plots the standard deviation of eddy kinetic energy field during summer (July–September). White color means the basin area where standard deviation of eddy kinetic energy less than $10\,cm^2\,s^{-2}$, or the shelf region where calculations were ignored due inaccurate tidal corrections.

176–171°W, implying that eddies occurred along the northern Aleutian Islands.

For 2002, a narrow band of high EKE variability with a width of about 80 km lay along the eastern shelf break similar to the one in 2001 (Fig. 3E). The magnitude of EKE variability near the Pribilof Islands was also small ($<60\,cm^2\,s^{-2}$). However, there was certainly generation and propagation of the eddy field. Major high EKE variability occurred near Amchitka Pass, Amukta Pass and off Zhemchug Canyon. In particular, the eddy field near Amukta Pass was broad and large magnitude, implying input of instability to the shelf break.

In 2003 (Fig. 3F), significantly high EKE variability was distributed widely from Pribilof Canyon to Zhemchug Canyon along the eastern shelf break. This high EKE band ranging from 30 to $300\,cm^2\,s^{-2}$ was found ~100–200 km offshore from the shelf break. Thus, extremely strong eddies appeared along the shelf break in the summer of 2003. Additionally, this high EKE band was located very close to the shelf break compared to previous years. Along the Aleutian Islands, high eddy activity was discovered alongshore, differing from 2001 and 2002.

We also examined original SLA plots. Sequential plots of SLA (not shown) indicate that stationary eddies exist along the Aleutian Islands between the Amchitka Pass and the Umnak Plateau, and that eddies propagate along the eastern shelf break from the Umnak Plateau (or near the Pribilof Canyon) to the Zhemchug Canyon. The northwestward propagation of eddies

along the eastern shelf break is consistent with the results of Okkonen (2001a) and Mizobata and Saitoh (2004).

In summary, there are significant differences in the EKE field in the Bering Sea basin for the six years presented. In 1998 and 1999, EKE was relatively weak. Small-scale eddies occurred along the Aleutian Islands, and fewer EKE perturbations appeared along the eastern shelf break in 1999. In 2000 and 2003, EKE perturbations emerged along the north side of the Aleutian Islands and along the eastern shelf break. In 2001 and 2002, EKE perturbations were revealed near the Aleutian passes and the eastern shelf break in the Bering Sea basin except for the Umnak Plateau.

To add further information about the movement of the eddy field along the eastern shelf break, a time-longitude plot of EKE (not the standard deviation of EKE) was made (Fig. 4). We extracted available EKE values nearest the eastern shelf break (Fig. 4, upper-right map). Black arrows in Fig. 4 indicate that the eddy field mostly propagated northwestwardly along the eastern shelf break (Okkonen, 2001a). In the summer of 1999, however, low eddy activity can be seen at the shelf break from 176°W to 172°W (Mizobata and Saitoh, 2004). In the summer of 2001 and 2002, there was relatively small magnitude of the eddy field between 174°W and 172°W (Fig. 4) resulting in low variability of EKE (Fig. 3D and E). Fig. 4 also shows the propagation of quite strong EKE field along the eastern shelf break during spring and summer in 2003.
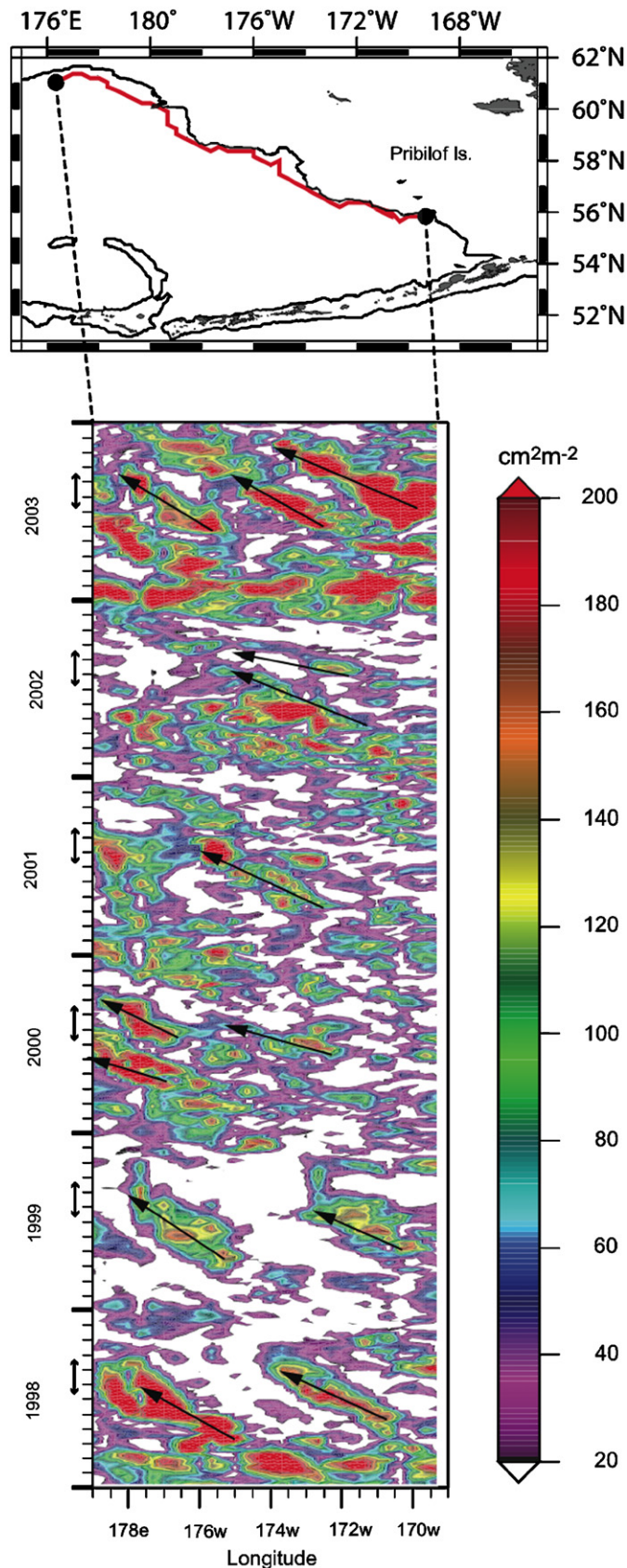
Fig. 4. Time-longitude plots of the eddy kinetic energy (EKE) along the eastern shelf break. Available EKE dataset nearest shelf break (1000-m isobath) was used. Red line inside upper-right maps shows the area where the data of EKE was extracted. Black arrows indicate northwestward propagation of eddies. Two-head arrows indicate the period from July to September.

3.2. Summer primary production in the euphotic zone (PP_{eu})

Fig. 5 shows the summer-averaged PP_{eu} distributions from 1998 to 2003. Interannual variability in PP_{eu} roughly corresponded to the variability of the eddy field shown in Fig. 3. For this discussion, we ignore PP_{eu} near the Alaskan coast, as coastal chl-a values probably include algorithm errors due to the high concentration of suspended sediment. Instead, we focus on productivity over the eastern shelf break, especially in the vicinity of the Pribilof Islands.

In 1998, high PP_{eu} ($>25\,\mathrm{g\,C\,m^{-2}\,month^{-1}}$) was distributed over the basin area (Fig. 5A). In particular, high PP_{eu} ($>40\,\mathrm{g\,C\,m^{-2}\,month^{-1}}$) appeared over Umnak Plateau, Pribilof Canyon and Zhemchug Canyon. A similar value or higher PP_{eu} was estimated around the Pribilof Islands. Along the Aleutian Islands, PP_{eu} was relatively high ($25\text{–}30\,\mathrm{g\,C\,m^{-2}\,month^{-1}}$), excluding the Aleutian passes.

In 1999, extremely low PP_{eu} ($\sim15\,\mathrm{g\,C\,m^{-2}\,month^{-1}}$) formed over the basin and along the eastern shelf break, except for over Umnak Plateau and near Pribilof Canyon (Fig. 5B). The few available data (due to cloudiness) indicate that there was low PP_{eu} ($<20\,\mathrm{g\,C\,m^{-2}\,month^{-1}}$) in the shelf area and a spotty distribution of high PP_{eu} at the western side of the Pribilof Islands. Along the Aleutian Islands, there was a low PP_{eu} area ($20\text{–}25\,\mathrm{g\,C\,m^{-2}\,month^{-1}}$) from Amchitka Pass to near Amukta Pass.

In 2000 (Fig. 5C), a high PP_{eu} band ($>25\,\mathrm{g\,C\,m^{-2}\,month^{-1}}$) formed along the eastern shelf break. High primary production occurred around Pribilof Canyon with a maximum value of $57\,\mathrm{g\,C\,m^{-2}\,month^{-1}}$ ($55.7°\mathrm{N}$, $169.7°\mathrm{W}$). At about $58°\mathrm{N}$ along the eastern shelf break, a high PP_{eu} band extended westward from Zhemchug Canyon to the deep basin. More than $30\,\mathrm{g\,C\,m^{-2}\,month^{-1}}$ PP_{eu} values were estimated around the Pribilof Islands, over the middle shelf ($57\text{–}58°\mathrm{N}$, $170\text{–}166°\mathrm{W}$) and along the Aleutian Islands. The distribution pattern of High PP_{eu} from Amchitka Pass to Amukta Pass was similar to that of high variability of EKE in 2000.

In 2001, a high PP_{eu} band extended from Umnak Plateau to Zhemchug Canyon (Fig. 4D). Values of more than $30\,\mathrm{g\,C\,m^{-2}\,month^{-1}}$ were found at the eastern shelf break west of the Pribilof Islands, with a maximum value of $59\,\mathrm{g\,C\,m^{-2}\,month^{-1}}$ ($56.3°\mathrm{N}$, $172.4°\mathrm{W}$), and at Umnak Plateau with a maximum value of $73\,\mathrm{g\,C\,m^{-2}\,month^{-1}}$ ($54.2°\mathrm{N}$, $167.7°\mathrm{W}$). PP_{eu} of more than $25\,\mathrm{g\,C\,m^{-2}\,month^{-1}}$ was widely distributed around and near Zhemchug Canyon ($56\text{–}59°\mathrm{N}$, $178\text{–}175°\mathrm{W}$). PP_{eu} at Amukta Pass was low, $<15\,\mathrm{g\,C\,m^{-2}\,month^{-1}}$, while higher PP_{eu} was found extending from Amchitka Pass into the deep basin ($52\text{–}55°\mathrm{N}$, $180\text{–}176°\mathrm{W}$).

In 2002, considerably high PP_{eu} ($\sim30\text{–}75\,\mathrm{g\,C\,m^{-2}\,month^{-1}}$) developed along the eastern shelf break from Umnak Plateau to Navarin Canyon, around the Pribilof Islands and along the Aleutian Islands between Amchitka Pass and Amukta Pass (Fig. 5E). An area of high PP_{eu} was distributed from the eastern shelf break between Zhemchug Canyon and Navarin Canyon leading into the basin ($58\text{–}60°\mathrm{N}$, $175°\mathrm{E}\text{–}178°\mathrm{W}$). A different PP_{eu} pattern with higher values surrounding a relatively low core emerged at $52\text{–}54°\mathrm{N}$ and $176\text{–}174°\mathrm{W}$, possibly indicating an eddy-like feature.

In 2003, a broad, high PP_{eu} band appeared along the shelf break. In particular, high PP_{eu} of over $50\,\mathrm{g\,C\,m^{-2}\,month^{-1}}$ was found from Umnak Plateau to Pribilof Canyon. From the Pribilof Islands to the eastern shelf break ($56\text{–}58°\mathrm{N}$, $175\text{–}170°\mathrm{W}$), there was a high-magnitude band of PP_{eu}, similar to 2002. Along the Aleutian Islands, a high productive area emerged close to the coast ($52\text{–}54°\mathrm{N}$, $176\text{–}174°\mathrm{W}$), showing a mesoscale pattern similar to 2002.
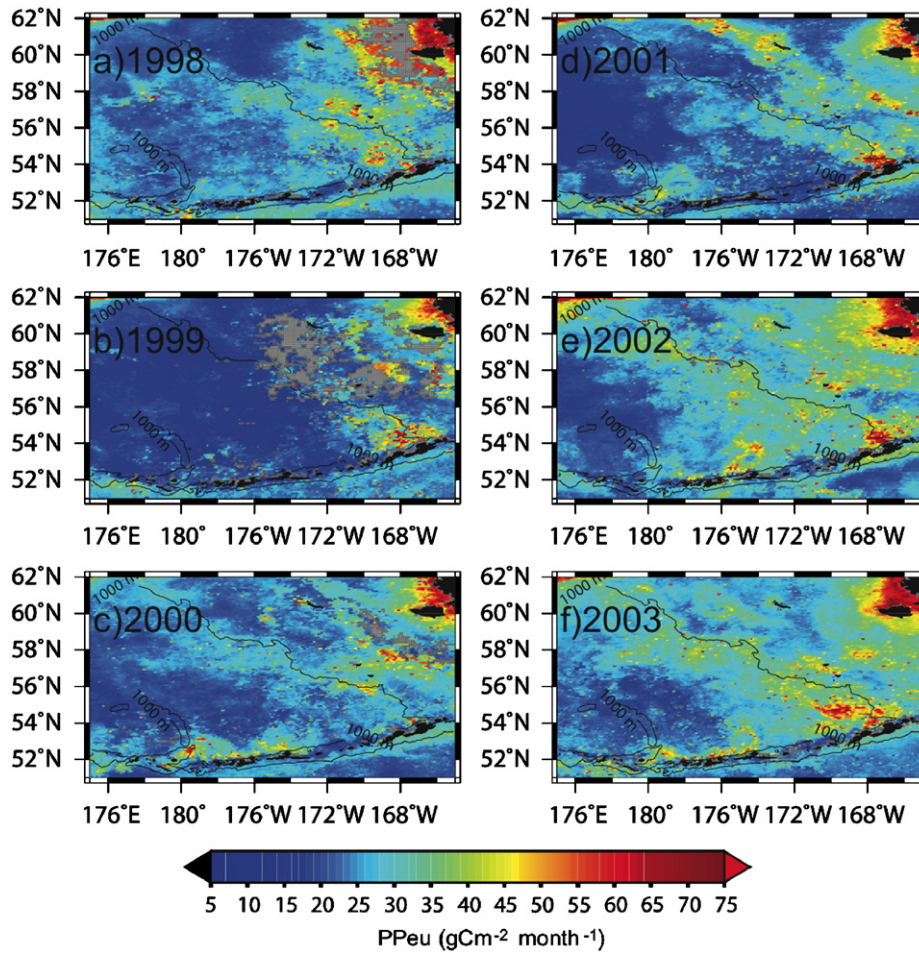
Fig. 5. Summer (July–September)-averaged primary production within the euphotic zone (PP_{eu}) in the eastern Bering Sea; the black contour line represents the 1000-m isobath.

3.3. Simulations of the eddy field and the on-shelf flux in the vicinity of the Pribilof Islands

The altimeter analysis in Section 3.1 indicated that perturbations emerged near the Aleutian passes and the eastern shelf break during 2000–2003, but there were fewer perturbations along the eastern shelf break during 1999. Therefore, to investigate the eddy field and on-shelf fluxes in both situations, we ran the ECOM-si from initial conditions with and without a barotropic, 200-km-wavelength perturbation. Hereafter, we refer to these model runs as the "perturbation case" and "non-perturbation case." Developments of the eddy field and on-shelf fluxes from both cases are shown in Fig. 6.

Mesoscale eddies along the shelf break were reasonably introduced by the perturbation case (Fig. 6A–C). Northeast is at the top of each panel, and the eastern Bering Sea shelf runs from right to left; Pribilof Canyon is at the upper right. At day 20, two anticyclonic eddies (solid lines) were generated at $X = 160$ km, $Y = 240$ km and $X = 310$ km, $Y = 220$ km, while two cyclonic eddies (dashed lines) were simulated at $X = 40$ km, $Y = 250$ km and $X = 280$ km, $Y = 260$ km (Fig. 6A). The average diameter of these eddies was about 90 km. An anticyclonic eddy also was found near Pribilof Canyon. Fig. 6 also shows the magnitude of net on-shelf fluxes (red bars) between 50 and 200 m water depth along the 200-m isobath. High on-shelf fluxes were estimated at $X = 100$–150 km and $X = 190$–200 km near the area between an anticyclonic eddy and a cyclonic eddy. Other on-shelf fluxes were between $X = 220$–480 km, including Pribilof Canyon. At day 30,

both anticyclonic eddies (solid lines) propagated offshore, then two cyclonic/anticyclonic eddy pairs were formed at $X = 10$–150 km and $X = 230$–320 km in the shelf break area. Near Pribilof Canyon, a large anticyclonic eddy was produced. High on-shelf fluxes were present at $X = 90$–130 km, likely due to cross-slope velocity components of a cyclonic eddy located at $X = 60$ km, $Y = 260$ km. Other high on-shelf fluxes occurred at the southern part of Pribilof Canyon ($X = 430$–450 km). The high fluxes also seemed to result from a large shelfward component of an anticyclonic eddy located at $X = 330$–460 km, $Y = 260$–350 km. At $X = 230$ km and $X = 280$–300 km, on-shelf fluxes were still present, but abated following the decay of a cyclonic eddy. At day 40, cyclonic eddies near the shelf break disappeared, and an anticyclonic eddy collapsed near Pribilof Canyon. Another anticyclonic eddy, however, remained about 20–30 km offshore at $X = 210$ km, $Y = 230$ km. On-shelf fluxes decreased markedly with the disappearance of eddies.

The non-perturbation case suppresses generation of large mesoscale eddies (Wang and Ikeda, 1997b) at the shelf break, except near Pribilof Canyon (Fig. 6D–F). Small-scale eddies, however, appeared at $X = 80$–310 km, $Y = 210$–290 km until day 20. A meander, which was generated at $X = 360$–460 km, $Y = 220$–310 km at day 10 (not shown) and propagated northwestward, generating small-scale eddies. At day 20, there was a large anticyclonic eddy near Pribilof Canyon ($X = 300$–480 km). High on-shelf fluxes were observed at $X = 110$ km and $X = 240$–300 km where the ridge of the jet flow approached the shelf break. Other high fluxes were found at the mouth of Pribilof
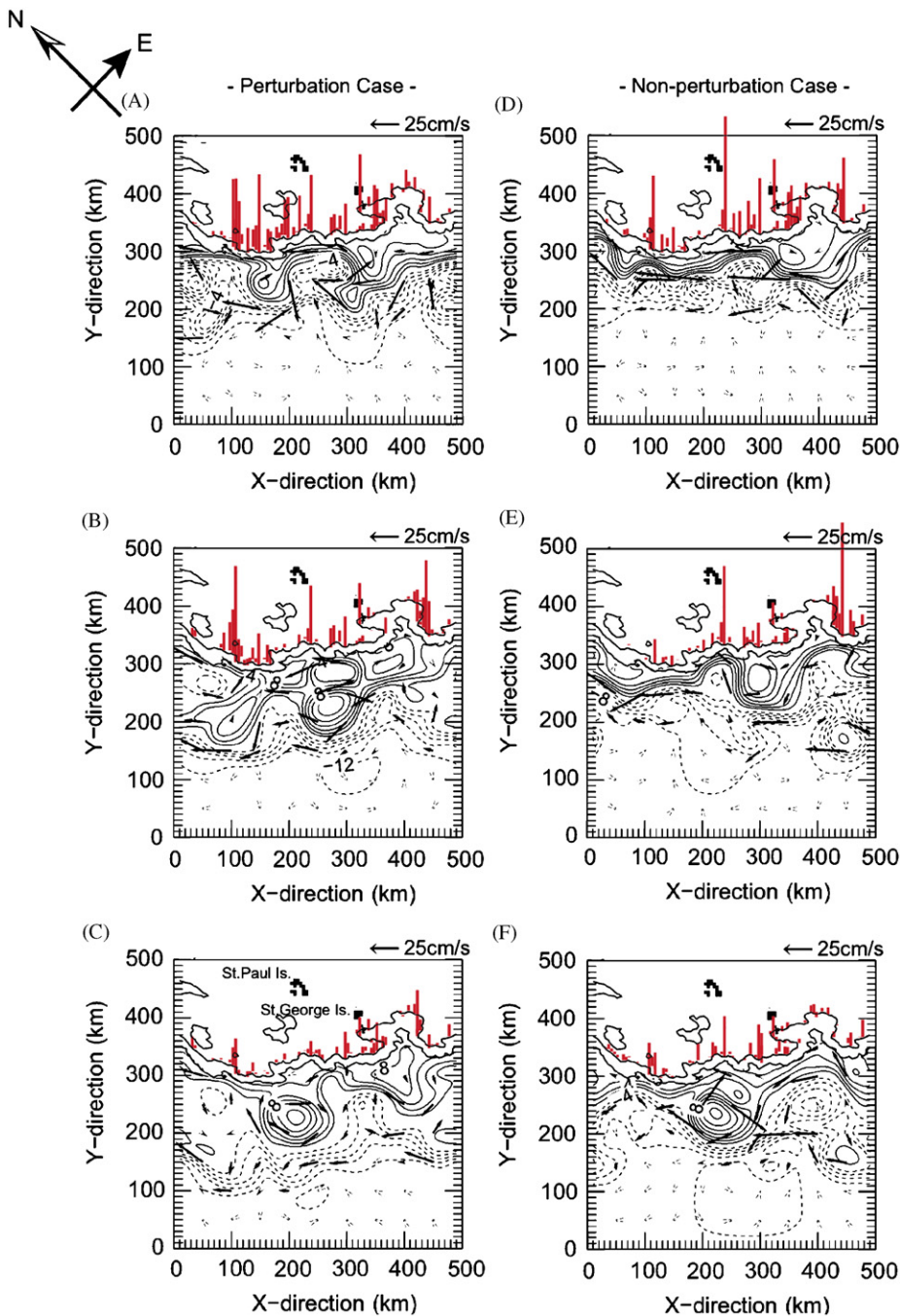
Fig. 6. Evolution of the eddy field in the "perturbation case" and "non-perturbation case"; solid and dashed contours represent positive and negative surface elevation (cm), respectively. The contour interval is 2 cm. Red bars indicate the amount of on-shelf flux along the 200-m isobath.

Canyon ($X = 340$–370 km and $X = 430$–450 km), due to an increase in the cross-slope velocity component by negative vorticity. By day 30, the small-scale eddies had decayed. On-shelf flux also was increased at the southern part of the Pribilof Canyon where the meander propagated northwestwardly, enhancing the cross-slope velocity component ($X = 450$ km, $Y = 360$ km). The large negative vortex split into two small anticyclonic eddies at day 25 (not shown). One propagated along the shelf break accompanied by a cyclonic eddy; the other, which can be seen at $X = 450$ km, $Y = 170$ km, moved offshore. At day 40, a cyclonic/anticyclonic eddy pair occurred at $X = 170$–300 km, $Y = 170$–310 km. The northwestward movement of an anticyclonic eddy resulted in a decrease in on-shelf fluxes at the southern part of

Pribilof Canyon and an increase in on-shelf fluxes at $X = 240$ km. A reduction of on-shelf flux occurred at $X = 110$ km due to detachment of the meander from the shelf beak. Another cyclonic eddy moved offshore following the separation of the jet flow from the shelf break near Pribilof Canyon. Some on-shelf fluxes were seen at $X = 100$–300 km between the cyclonic and anticyclonic eddies which is related to the cross-shelf component of the eddy pair. Around Pribilof Canyon, on-shelf fluxes diminished due to the detachment of the jet from the shelf break.

Fig. 7 illustrates the time series of on-shelf fluxes from 50 to 200 m water depth for the whole model domain and for an area just around Pribilof Canyon for both perturbation and non-perturbation cases. Net on-shelf flux was maintained when the
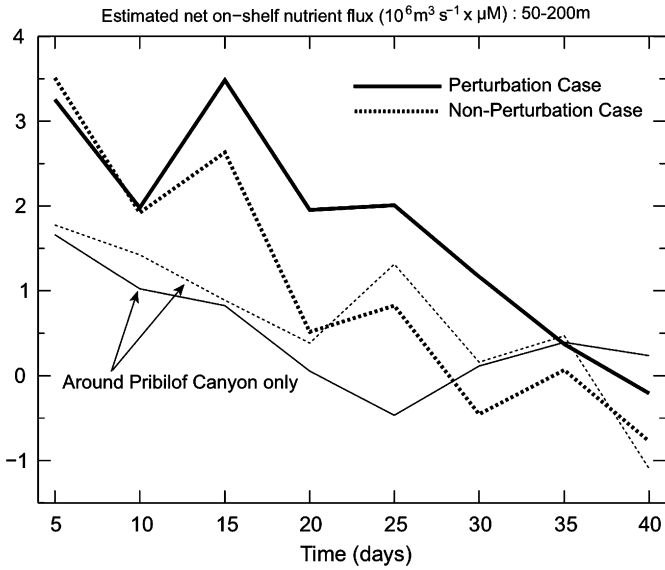
Fig. 7. Time series of the amount of net on-shelf flux from 50 to 200 m water depth at the 200-m isobath within the model domain (thick line) and around Pribilof Canyon (thin line); solid and dashed lines indicate the "perturbation case" and "non-perturbation case", respectively.

Table 1
Summary of the numerical experiments

	Perturbation case		Non-perturbation case	
	0–50 m	50–200 m	0–50 m	50–200 m
On-shelf nutrient flux ($\times 10^6$ m^3 s^{-1} μM)	6.30 (1.31)	45.78 (16.89)	4.30 (1.57)	41.94 (18.36)
Off-shelf nutrient flux ($\times 10^6$ m^3 s^{-1} μM)	3.98 (0.66)	31.77 (13.05)	4.79 (0.77)	33.70 (13.03)
Net on-shelf nutrient flux ($\times 10^6$ m^3 s^{-1} μM)	2.31 (0.65)	14.01 (3.84)	−0.50 (0.80)	8.24 (5.33)
On-shelf transport (Sv)	3.35 (1.30)	5.47 (2.52)	2.85 (1.29)	5.13 (2.58)
Off-shelf transport (Sv)	2.61 (0.85)	4.33 (1.81)	2.56 (0.74)	4.40 (1.67)
Net on-shelf transport (Sv)	0.75 (0.45)	1.13 (0.71)	0.29 (0.56)	0.74 (0.92)
			50–200 m	0–200 m
Increase in net on-shelf nutrient flux (%)			69.94	110.72
Increase in net on-shelf transport (%)			54.09	82.38

On-/off-shelf nutrient flux ($\times 10^6$ m^3 s^{-1} μM) and transport (SV = 10^6 m^3 s^{-1}) in both cases are shown. Numbers in parentheses indicate flux or transport only around Pribilof Canyon. The lower part of the table also shows a rate of increase in on-shelf flux and transport by the evolution of the eddy field, comparing the perturbation case with the non-perturbation case.

eddy field developed between days 20 and 25 and suddenly decreased following the decay of the eddy field in the perturbation case. Conversely, Fig. 7 shows little difference in the amount of on-shelf flux around Pribilof Canyon. A slight difference from days 25 to 35 in the non-perturbation case was caused by the jet approaching Pribilof Canyon.

Table 1 summarizes results of numerical simulations. Basically, on-/off-shelf nutrient flux below 50 m water depth is larger than that between 0 and 50 m water depth in both cases, because we introduced tracer beneath $\sigma = -0.115$ in the basin. There is also small on-/off-shelf flux in the surface layer (0–50 m water depth), which indicates that upwelled nutrient in the surface layer of the basin was advected to the shelf area, while most of nutrients are directly advected from the subsurface layer of the basin to the upper 50 m water column in the shelf. Our tracer experiments indicate that the development of large eddy fields leads to a 9.1%

increase in on-shelf fluxes, a ~5.7% decrease in off-shelf fluxes, and a ~69.9% increase in net on-shelf fluxes from 50 to 200 m water depths over the whole model domain. In both cases, positive net on-shelf transport was estimated between 0 and 200 m water depths. The evolution of the eddy field contributes to a ~54% increase in net on-shelf transport below the 50 m water depth over the model domain (Table 1). Around the Pribilof Canyon, however, larger on-shelf flux and transport were estimated in the non-perturbation case, compared to those in the perturbation case. These imply that the evolution of the eddy field induces the magnitude of on-shelf fluxes and suppresses that of off-shelf fluxes at the shelf break simultaneously, except for the Pribilof Canyon. If fluxes around Pribilof Canyon are excluded, then there is a 149.2% increase in net on-shelf flux at the shelf break, compared to the small-eddy-induced flux.

3.4. Three-dimensional isotherms and fluorescence distribution at Pribilof Canyon

Hydrographic observations using a towed vehicle revealed high fluorescence distributed above the layer between the 5 and 7 °C isotherms (Fig. 8). At the Bering Sea shelf break of depth from 50 to 200 m, temperatures between 5 and 7 °C almost correspond to the pycnocline (Mizobata et al., 2002). High fluorescence of more than 20 μg L^{-1} appeared at 56.2°N along the 169.8°W meridian, between 55.8°N and 56.3°N along the 169.6°W meridian, between 55.9°N and 56.2°N along the 169.4°W meridian, and between 55.8°N and 56.2°N along the 169.2°W meridian. Those horizontal distributions of high fluorescence nearly coincided with the area between the 200- and 1000-m isobaths. Most of the high fluorescence distributions were found from the surface to 30 m water depth. A thin layer of high fluorescence also existed at 56.1°N along the 169.8°W meridian, at 56.2°N along the 169.6°W meridian, and at 55.9–56.05°N along the 169.2°W meridian. The thin layer of fluorescence occurred above the area where isotherms were tilted upwards toward the shelf. There was no fluorescence at 55.8°N, 169.8°W and 55.8°N, 169.4°W, where isotherms were depressed. This indicates that the
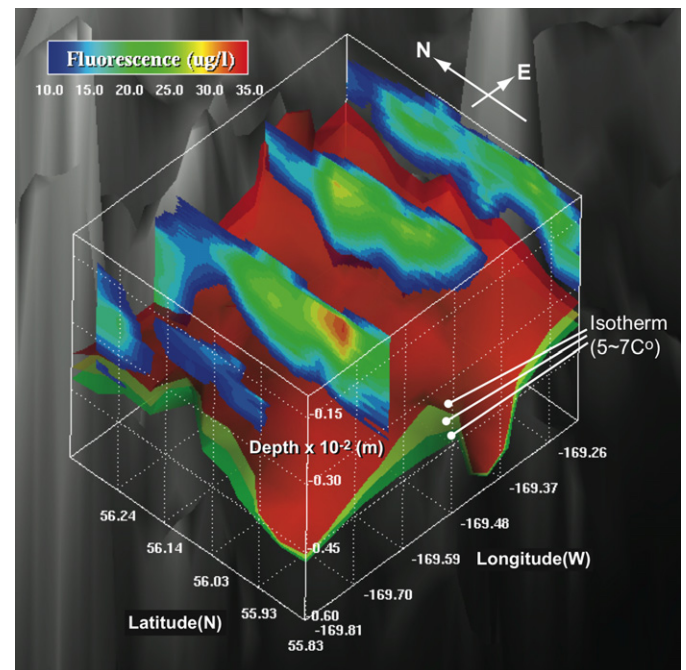

Fig. 8. Three-dimensional structure of isotherms (green = 5 °C, yellow = 6 °C, red = 7 °C) and high fluorescence at Pribilof Canyon on 26 July 2003.

vertical water structure caused by mesoscale eddies regulates distribution of phytoplankton at the shelf break (Wang and Ikeda, 1997a).

4. Discussion

4.1. Origins of variability in the eddy field

The simulations of the eddy field in Section 3.3 demonstrated that the BSC instability excited mesoscale eddies quickly and increased the number of eddies along the eastern shelf break in the vicinity of the Pribilof Islands (Fig. 6). The prescribed instability perturbation (Eq. (8)) in the numerical experiments was assumed to be initiated near the Umnak Plateau when the ANSC turns northwestward, forming the BSC. The summer eddy field showed high EKE variability along the Aleutian Islands, around Umnak Plateau, and along the eastern shelf break in 1998, 1999, 2000 and 2003 (Fig. 3A–C, F). These examples suggest that the instability perturbation was triggered along the ANSC/BSC system. On the other hand, Fig. 3 also revealed that high EKE variability near the Aleutian passes extended to the basin or the eastern shelf break in the summer of 2001 and 2002 (Fig. 3D and E). The patterns formed by those years' EKE deviations indicate that the baroclinic perturbation propagated from the flows through the Aleutian passes to the eastern shelf break via the basin, eventually contributing to generation of the eddy field along the eastern shelf break. Okkonen (1996) showed that EKE variability near the Aleutian passes is due not only to the ANSC, but also to inflow through the Aleutian passes affecting the ANSC.

An increase of the inflow through the Aleutian passes is induced by the eddy/meander, position and strength of the Alaskan Stream (Okkonen, 1996; Stabeno et al., 2005). According to Okkonen (1996), maximum inflow into the Bering Sea basin through Amchitka Pass occurs when the center of an Alaskan Stream eddy is located nearest the axis of Amchitka Pass. From 2000 to 2002, extremely high EKE variability was shown south of Amchitka Pass. Thus, there should have been an increase in the inflow of North Pacific (NP) water through the Aleutian passes during that time. An increase in inflow of the NP water characterized by high temperature/high salinity will lead the baroclinic instability between the Bering Sea shelf and the basin, because the Bering Sea shelf water is defined by its relatively low temperature/low salinity due to dynamics of the seasonal sea-ice zone. Conversely, low EKE variability along the northern side of the Aleutian Islands in 1999 implied a relatively small amount of inflow through the Aleutian passes, resulting in less baroclinic instability along the eastern shelf break. Thus, our results suggest two factors affecting the eddy field along the shelf break. One is the instability from the ANSC/BSC system or the Aleutian passes, and the other is the baroclinic instability induced by the inflow of the NP water through the passes.

Mizobata and Saitoh (2004) hypothesized that the Aleutian Low (a seasonal composite of atmospheric pressure) can strengthen the transport of the Alaskan Stream, the ANSC and the BSC, resulting in high EKE variability along the Aleutian Islands and the Bering Sea eastern shelf break, based on Hollowed and Wooster (1992), who proposed that the strong Aleutian low pressure reinforces the Alaskan Stream. Actually, the Aleutian Low was weak in the winter of 1999, implying weak advection of the Alaskan Stream, and relatively strong in 2000 (Mizobata and Saitoh, 2003). In situ, observations measured an increase in transport of the ANSC and BSC systems (assuming a reference level of 1500 dbar or the bottom) during 2000 (P.J. Stabeno, personal communication). Our analysis also showed high variability of the eddy field from 2000. Additionally, Melsom et al.

(1999) presented a linkage between the number/strength of eddies and the El Niño-Southern Oscillation, via coastal Kelvin waves and atmospheric teleconnections in the eastern Gulf of Alaska. However, it takes 2 or 3 years for an eddy in the Alaskan Stream to propagate from the eastern Gulf of Alaska to the central Aleutians (Okkonen et al., 2001b). At this time, it is unclear how climatic forcing affects the increase in the inflow of the NP water. In the future, we will apply an Air–Ice–Ocean coupled model to the Bering Sea and the North Pacific to learn more about climatic forcing of those marine systems.

4.2. Enhancement of on-shelf flux and primary production by mesoscale eddies

Numerical simulations of the eddy field showed that on-shelf fluxes can occur along the 200-m isobath below 50 m water depth (Fig. 6). The evolution of the eddy field resulted in a 69.9% increase (whole model domain) and a ~149% increase (except for around Pribilof Canyon) of the net on-shelf flux (Table 1). There are some complex processes at the Pribilof Canyon. The large cross-slope component of the current velocity enhanced the amount of the net on-shelf flux, when an eddy/meander propagated along or approached the shelf break (Fig. 6). Moreover, the northwestward propagation of the eddy field along the eastern shelf break is implied by the altimeter data analysis (Fig. 4). Thus, on-shelf nutrient flux will be enhanced by the eddy field along the shelf break. At the Pribilof Canyon, however, the magnitude of cross-slope velocity is small due to relatively long distance between eddy/meander and the shelf break resulting from the topographic feature. Thus, the evolution of the eddy field does not contribute to an increase of the net on-shelf flux at Pribilof Canyon.

At the shelf break, the "shelf break front" stabilizes the water column and retains the phytoplankton within the euphotic zone during summer (Gawarkiewicz and Chapman, 1992; Springer et al., 1996). Around Pribilof Canyon, observations from a towed CTD/fluorometer revealed high fluorescence in the stable water column (surface—30 m water depth) defined by the 5–7 °C isotherms (Fig. 8) when an anticyclonic eddy propagated northwestward near the canyon. The high fluorescence distribution was consistent with the area between the 200- and 1000-m isobaths where on-shelf fluxes result from the passage of mesoscale eddies along the shelf break (Figs. 5 and 7). In this case, there was a low level of on-shelf flux and the stable water column maintained high fluorescence. Conversely, the eddy-induced on-shelf flux and stable water column can lead to a high biomass of phytoplankton at the shelf break. The estimated PP_{eu} field illustrated high productivity areas ($>30 \, g \, C \, m^{-2} \, month^{-1}$) along the shelf break, corresponding to the high EKE variability areas (Figs. 3C–F and 4C–F). In particular, there was extremely high PP_{eu} over the shelf break and the basin in 2002 and 2003. In contrast, our satellite data analyses indicate low PP_{eu} and low EKE variability at the shelf break area and the basin in 1999. As a matter of course, the apparent interannual variability of PP_{eu}, will result, in part, from uncertainties in estimation of summer monthly PP_{eu}, which was mentioned in Section 2.2. Actually, there was heavy cloud cover in the Bering Sea basin area, which can lead to an underestimation of chl-a and PP_{eu}, especially in 1999. However, our numerical simulations and hydrographic surveys suggest that the coincidence of the magnitude of PP_{eu} with that of EKE variability indicates the close relationship between the PP_{eu} and the eddy field at the shelf break during those summers.

There can be a contribution to PP_{eu} from not only on-shelf flux, but also basin-ward transport of eddies. During spring, Okkonen et al. (2004) observed high chl-a concentrations associated with an anticyclonic eddy along the Bering Sea shelf break.

They suggested that the eddy entrained chlorophyll from the shelf, discharged it to the basin, and expanded the Bering Sea Green Belt. Basin-ward transport of chlorophyll by eddies is more effective during summer, when PP_{eu} is generally high at the shelf break. Moreover, offshore movement of eddies was observed near Pribilof Canyon in 2000, and this offshore movement also can transport highly productive water to the basin.

In 1998, 2000, 2001, 2002 and 2003, high primary production appeared along the shelf west of the Pribilof Islands (Fig. 5A, C, D and F). Generally, PP_{eu} in the Bering Sea shelf region is low after the spring bloom (April–June); so this area seems to be a hotspot for the ecosystem. There is a possibility of underestimating primary production due to heavy cloud in 1999. However, we believe that PP_{eu} at the shelf and shelf break in 1999 was lower than those in other years, because low PP_{eu} area ($<20\,g\,C\,m^{-2}$ month^{-1}) can be seen at northwest and south of Pribilof islands and basin area. In this area, a shelfward-directed nutrient supply was implied by a drifting buoy study by Mizobata and Saitoh (2003), and the on-shelf flux was estimated by numerical simulations (Fig. 6). The eddy-induced on-shelf flux probably contributes to the high productivity at the western shelf of the Pribilof Islands. Additionally, Kowalik and Stabeno (1999) predicted anticyclonic tidal residual currents of 10–15 cm s^{-1} around the Pribilof Islands from a tidal model. The anticyclonic tidal current promotes the maintenance of a frontal system around the islands resulting in upwelling events/downwelling event (Kowalik and Stabeno, 1999). A previous drifting buoy did not show that surface flow reached around the Pribilof Islands, but there is the possibility of nutrient transport from the basin around the Pribilof Islands by the coupling effect of on-shelf flux and tidal motion.

In this study, we combined satellite data analyses, numerical modeling and the results of hydrographic measurements to elucidate the interannual variability of summer PP_{eu} related to mesoscale eddies and the resulting on-shelf nutrient flux. But poorly known issues, which remain here, are daily-/small-scale primary productivity in the Bering Sea shelf break and basin area. To clarify these issues, we need to conduct frequent monitoring of these regions in the vicinity of the Pribilof Islands (on a daily basis, if possible) by ship surveys and satellite measurements.

5. Conclusions

Our analyses of satellite-derived altimetry and chl-a, estimates of EKE and on-shelf fluxes using a numerical model, and observations from a towed vehicle, allow us to formulate the following conclusions regarding mesoscale eddies and enhancement of productivity:

(1) Interannual variation in PP_{eu} field is positively related to that in the eddy field over the Bering Sea's eastern shelf break during summer. From 2000 to 2003, when high eddy activity was found, high primary production was maintained in the area. In particular, a stronger eddy field and wide-ranging, high PP_{eu} occurred in 2003. Conversely, there was low EKE variability and low PP_{eu} in 1999.
(2) There are two possible mechanisms for exciting mesoscale eddies along the eastern shelf break:
  (a) Perturbations from the Aleutian passes, such as in 2001 and 2002;
  (b) Inflow of the NP waters through the Aleutian passes, enhancing the ANSC/BSC jet flow, which results in stronger instability, such as in 2000 and 2003. In 1999, there was low instability along the northern Aleutian Islands and the Bering Sea deep basin, leading to low EKE variability along the eastern shelf break.
(3) A numerical model has been used to reproduce eddies, on-shelf fluxes and perturbations propagated from the Aleutian passes. Under the perturbation case, stronger, longer lasting, larger mesoscale eddies and larger net on-shelf fluxes were produced, while small mesoscale eddies and small net on-shelf fluxes were produced under the non-perturbation case. Thus, our results suggest that perturbations from the Aleutian passes can affect the remote eddy field and on-shelf fluxes along the Bering Sea's eastern shelf break.
(4) Eddy-induced on-shelf flux can enhance primary production at the eastern shelf break, helping to maintain the Green Belt, which usually lasts from spring to summer.
(5) While this study focuses on the Bering Sea shelf break area, the basic physics is same in all shelf break area in the world. Thus, our results are likely generally applicable to all shelf break area domains in which propagating eddies are found.

References

Arakawa, A., Lamb, V.R., 1977. Computational design of the basic dynamic processes of the UCLA general circulation model. In: Chang, J.C. (Ed.), General Circulation Models of the Atmosphere. Academic Press, New York, pp. 173–265.
Behrenfeld, M.J., Falkowski, P.G., 1997. Photosynthetic rates derived from satellite-based chlorophyll concentration. Limnology and Oceanography 42, 1–20.
Blumberg, A.F., 1991. A primer for ECOM-si. Technical Report, HydroQual, Inc., Mahwah, NJ, p. 66.
Casulli, V., 1990. Semi-implicit finite-difference methods for the two-dimensional shallow water equations. Journal of Computational Physics 86, 56–74.
Ciannelli, L., Brodeur, R.D., Swartzman, G.L., Salo, S., 2002. Physical and biological factors influencing the spatial distribution of age-0 walleye pollock (Theragra chalcogramma) around the Pribilof Islands, Bering Sea. Deep-Sea Research II 49 (26), 6,109–6,126.
Gawarkiewicz, G., Chapman, D.C., 1992. The role of stratification in the formation and maintenance of shelfbreak front. Journal of Physical Oceanography 22, 753–772.
Hollowed, A.B., Wooster, W.S., 1992. Variability of winter ocean conditions and strong year classes of northeast Pacific groundfish. ICES Marine Science Symposia 195, 433–444.
Johnson, G.C., Stabeno, P.J., Riser, S.C., 2004. The Bering Slope Current system revisited. Journal of Physical Oceanography 34, 384–398.
Kameda, T., Ishizaka, J., 2005. Size-fractionated primary production estimated by a two-phytoplankton community model applicable to ocean color remote sensing. Journal of Oceanography 61, 663–672.
Kinder, T.H., Coachman, L.K., Galt, J.A., 1975. The Bering Slope Current system. Journal of Physical Oceanography 5, 231–244.
Kowalik, Z., Stabeno, P.J., 1999. Trapped motion around the Pribilof Islands in the Bering Sea. Journal of Geophysical Research 104, 25667–25684.
Le Traon, P.-Y., Nadal, F., Ducet, N., 1998. An improved mapping method of multisatellite altimeter data. Journal Atmospheric and Oceanic Technology 15, 522–534.
Liu, H., Suzuki, K., Minami, C., Saino, T., Watanabe, M., 2002. Picoplankton community structure in the subarctic Pacific Ocean and the Bering Sea during summer 1999. Marine Ecology Progress Series 237, 1–14.
Mellor, G.L., Yamada, T., 1982. Development of a turbulence closure model for geophysical fluid problems. Review Geophysics and Space Physics 20 (4), 851–875.

Melsom, A., Meyers, S.D., O'Brien, J.J., Hurlburt, H.E., Metzger, J.E., 1999. ENSO effects on Gulf of Alaska eddies. Earth Interactions 3, 1–30 (Available at http://EarthInteractions.org.).

Mizobata, K., Saitoh, S., 2003. Characteristics of cyclonic and anticyclonic eddies in the southeastern Bering Sea 1998–2000 using TOPEX/Poseidon. Ocean Remote Sensing and Applications, The International Society for Optical Engineering, Proceedings of SPIE, vol. 4892, Bellingham, WA, USA, pp. 473–481.

Mizobata, K., Saitoh, S., 2004. Variability of Bering Sea eddies and primary productivity along the shelf edge during 1998–2000 using satellite multi-sensor remote sensing. Journal of Marine Systems 50, 101–111.

Mizobata, K., Saitoh, S., Shiomoto, A., Miyamura, T., Shiga, N., Toratani, M., Kajiwara, Y., Sasaoka, K., 2002. Bering Sea cyclonic andanticyclonic eddies observed during summer 2000 and 2001. Progress in Oceanography 55, 65–75.

Mizobata, K., Wang, J., Saitoh, S., 2006. Eddy-induced cross-slope exchange maintaining summer high productivity of the Bering Sea shelf break, Journal of Geophysical Research, 111, C10017, doi:10.1029/2005JC003335.

Morel, A., Berthon, J.F., 1989. Surface pigments, algal biomass profiles and potential production of the euphotic layer: relationships re-investigated in view of remote sensing applications. Limnology and Oceanography 34 (8), 1545–1562.

Okkonen, S.R., 1996. The influence of an Alaskan Stream eddy on flow through Amchitka Pass. Journal of Geophysical Research 101, 8839–8851.

Okkonen, S.R., 2001a. Altimeter observations of the Bering Slope Current eddy field. Journal of Geophysical Research 106, 2465–2476.

Okkonen, S.R., Jacobs, G.A., Metzger, E.J., Hurlburt, H.E., Shriver, J.F., 2001b. Mesoscale variability in the boundary currents of the Alaska Gyre. Continental Shelf Research 21, 1219–1236.

Okkonen, S.R., Schmidt, G.M., Cokelet, E.D., Stabeno, P.J., 2004. Satellite and hydrographic observations of the Bering Sea 'Green Belt'. Deep-Sea Research II 51, 1033–1051.

O'Reilly, J.E., Maritorea, S., O'Brien, M.C., Siegel, D.A., Toole, D., Menziers, D., Smith, R.C., Mueller, J.L., Mitchell, B.J., Kahru, M., Chavez, F.P., Strutton, P., Cota, G.F., Hooker, S.B., McClain, C.R., Carder, K.L., Muller-Karger, F., Harding, L., Magnuson, A., Phinney, D., Moore, G.F., Aiken, J., Arrigo, K.R., Letelier, R., Culver, M., 2000. In: Hooker, S.B., Firestone, E.R. (Eds.), SeaWiFS Postlaunch Calibration and Validation Analyses, Part 3. SeaWiFS Postlaunch Technical Report Series, NASA/TM-2000-206892, vol. 11.

Reed, R.K., Stabeno, P.J., 1999. The Aleutian North Slope Current. In: Loughlin, T.R., Ohtani, K. (Eds.), Dynamics of the Bering Sea. University of Alaska Sea Grant Press, pp. 177–191 AK-SG-99-03.

Robinson, I.S., 2004. Measuring the Oceans from Space, the Principles and Methods of Satellite Oceanography. Springer, Chichester, UK.

Roden, G.I., 1995. Aleutian Basin of the Bering Sea: thermohaline, oxygen, nutrient, and current structure in July 1993. Journal of Geophysical Research 100 (C7), 13,539–13,554.

Sapozhnikov, V.V., 1993. Influence of mesoscale anticyclonic eddies on the formation of hydrochemical structures in the Bering Sea. Oceanology (English Translation) 33, 299–304.

Schumacher, J.D., Stabeno, P.J., 1994. Ubiquitous eddies of the eastern Bering Sea and their coincidence with concentrations of larval pollock. Fisheries Oceanography 3, 182–190.

Shiomoto, S., Saitoh, S., Imai, K., Toratani, M., Ishida, Y., Sasaoka, K., 2002. Interannual variation in phytoplankton biomass in the Bering Sea basin in the 1990s. Progress in Oceanography 55, 147–163.

Smagorinsky, J., 1963. General circulation experiments with the primitive equations. I. The basic experiment. Monthly Weather Review 91, 99–164.

Springer, A.M., McRoy, C.P., Flint, M.V., 1996. The Bering Sea Green Belt: shelf edge processes and ecosystem production. Fisheries Oceanography 5, 205–223.

Stabeno, P.J., van Meurs, P., 1999. Evidence of episodic on-shelf flow in the southeastern Bering Sea. Journal of Geophysical Research 104, 29715–29720.

Stabeno, P.J., Schumacher, J.D., Ohtani, K., 1999. The physical oceanography of the Bering Sea. In: Loughlin, T.R., Ohtani, K. (Eds.), Dynamics of the Bering Sea. University of Alaska Sea Grant Press, pp. 1–28 AK-SG-99-03.

Stabeno, P.J., Kachel, D.G., Kachel, N.B., Sullivan, M.E., 2005. Observations from moorings in the Aleutian Passes: temperature, salinity and transport. Fisheries Oceanography 14, 39–54.

Sukahanova, I.N., Semina, J.H., Venttsel, M.V., 1999. Spatial distribution and temporal variability of phytoplankton in the Bering Sea. In: Loughlin, T.R., Ohtani, K. (Eds.), Dynamics of the Bering Sea. University of Alaska Sea Grant Press, pp. 453–483 AK-SG-99-03.

Swartzman, G., Napp, J., Brodeur, R.D., Winter, A., Ciannelli, L., 2002. Spatial patterns of pollock and zooplankton distribution in the Pribilof Islands, Alaska nursery area and their relationship to pollock recruitment. ICES Journal of Marine Science 59 (6), 1,167–1,186.

Wang, J., 1996. On global stability of the 2-D shallow water equations: an application of the root's distributive theorem for polynomials in the unit circle. Monthly Weather Review 124, 1301–1310.

Wang, J., Ikeda, M., 1995. Stability analysis of finite difference schemes for inertial oscillations in ocean general circulation models. In: Brebbia, C.A., Traversoni, L., Wrobel, L.C. (Eds.), Computer Modeling of Seas and Coastal Regions. Computational Mechanics Publications Southampton, Boston, pp. 19–27.

Wang, J., Ikeda, M., 1997a. A 3D ocean general circulation model for mesoscale eddies—II: Diagnostic analysis. Acta Oceanologica Sinica 16, 29–43.

Wang, J., Ikeda, M., 1997b. Diagnosing ocean unstable baroclinic waves and meanders using the quasigeostrophic equations and Q-vector method. Journal of Physical Oceanography 27, 1158–1172.

Wang, J., Ikeda, M., 1997c. Inertial stability and phase error of time integration schemes in ocean general circulation models. Monthly Weather Review 125, 2316–2327.